15 August 1969, Volume 165, Number 3894 SCIENCE

Lunar and Planetary Mass Concentrations

Mascons beneath large circular basins may explain dynamical asymmetries in the moon, Mars, and Mercury.

Brian T. O'Leary, Malcolm J. Campbell, Carl Sagan

Classical astronomical information on the figures of the moon and the terrestrial planets is now being supplemented by new data obtained from space vehicles. The optical figure and moments of inertia of these bodies are potentially rich sources of clues on the early history of the solar system. For example, dense lumps formed near the surface of Earth in the final stages of its accretion would long ago have been removed by isostatic compensation—a process which, it has recently been suggested (*1*), occurs because of partial melting in the low-velocity zone of Earth's upper mantle. But the existence of such a zone is closely connected with the thermal history of Earth. On planets with a history of more limited heating, such primordial inhomogeneities may have survived to the present epoch. In this paper we are concerned with drawing such connections and detailing the relation between figure and inhomogeneities for the moon, Mercury, Venus, Mars, and Earth. In all of the following discussion—because of either limitations in the models or poor resolution—we are concerned only with large-scale optical and gravitational features; correlation of the small-scale features lies in the future.

The authors are affiliated with the Center for Radiophysics and Space Research at Cornell University; Dr. Sagan is director of the Center's Laboratory for Planetary Studies.

State of the Observations

The moon and Mars (and perhaps Mercury) exhibit disequilibrium dynamical figures. In particular, the differences among their moments of inertia depart significantly from expected values. In the case of the moon, observations have firmly established that, of the moments of inertia (*2*), $C > B > A$, and that their differences are much greater than would be predicted from hydrostatic equilibrium and tidal theory (*3–6*). The following suggestions have been advanced to explain this discrepancy: a fossil tidal bulge of about 1 km resulting from solidification of the moon when it was closer to Earth (*7*), convection currents in the lunar interior (*8*), thermoelastic effects (*9*), and primeval density inhomogeneities (*10*).

But each of these suggestions encounters difficulties. The fossil tidal bulge cannot explain the asymmetry in C and B (*11*), and limb observations at various librations show no evidence for a fossil tidal bulge; in fact, there is some suggestion of a bulge of about 1 km inclined 35° to the axis of rotation, which operates in the wrong sense to explain the moments of inertia (*12, 13*). On the other hand, Runcorn and Shrubsall (*8*) report a geometric bulge toward Earth and propose convection currents in the interior as the cause. But this hypothesis runs into problems of viscous damping by convective flow (*13, 14*). The thermoelastic mechanism has also been criticized (*9, 13*), and it too requires a geometric bulge toward Earth. In all events it is clear from the lack of any agreement among optical observers (*8, 12, 13*) that the moon's external shape is not well established. The absence of a geometric bulge toward Earth is suggested by radar observations near the sub-Earth point (*13*). Moreover, large-scale geometric asymmetries are probably not major contributors to the dynamical asymmetries for reasons we discuss below. In regard to density inhomogeneities, Urey *et al.* (*15*) suggest that, in order to account for the differences in moments of inertia, 10^4 to 10^5 objects of varying density participated in the moon's formation. MacDonald (*5*) has revised this figure to $\lesssim$ 1000. On the other hand, O'Keefe and Cameron (*16*) argue that it would be impossible for random lumps to move the lunar center of gravity $\sim$ 1 km north of its geometric center, as suggested from observations.

For Mars, the advance of the line of apsides of Phobos and the regression of the nodes of Phobos and Deimos indicate a dynamical flattening of 0.0052 (*17*), close to the upper limit of 0.0057 given by Darwin-Radau theory for a planet in hydrostatic equilibrium. On the other hand, the optical oblateness is much greater, 0.0117 according to a recent measurement by Dollfus (*18*), or 0.0105, a weighted mean of the best observations of all observers (*19*). The latter value corresponds to a difference between equatorial and polar radii of 35 km; the corresponding difference derived under the assumption of hydrostatic equilibrium from the dynamical flattening is 17 km.

The possibility that the discrepancy is due to an equatorial layer of haze (*20*) has been criticized (*21*) on the ground that it could not affect the oblateness as measured by Wright's method of following surface features crossing the disk. There is an attendant difficulty in that the haze should be more prominent in observations made in blue rather than red light, but the oblateness is wavelength-independent (*22*). Furthermore, the haze must be restricted to the troposphere; but the tropopause lies very near the surface at Martian dawn and dusk (*23*). Urey (*24*) has proposed that the discrepancy can be explained by equatorial continental blocks in isostatic equilibrium, a suggestion supported by Sagan and Pollack (*25*), who argue on the basis of radar data and other considerations that there indeed may be such equatorial highlands. However, a difference of mean elevation (with respect to the "geoid") between equatorial and polar regions of 18 km (35 km − 17 km) corresponds to a difference of a factor of 6 in surface atmospheric pressure. Despite the vagaries of differential pressure measurements derived from spectrometric study of Mars, it does not seem that such an effect could have been overlooked, and Sagan and Pollack suggested that equatorial highlands do not explain the entire discrepancy. Should the measurements of optical oblateness be in serious error, the fact remains that a reasonable hydrostatic model for Mars must have a dynamical flattening considerably smaller than that observed. This closely parallels the case of the moon.

In the case of the planet Mercury, it has been proposed (*26*) that a permanent asymmetry of the gravitational potential in the equatorial plane is required to explain a direct rotation with a period precisely two-thirds of its orbital period, where the long axis of the asymmetry would point toward the sun at each perihelion passage. Liu (*27*) suggests that the bulge is due to differential thermal expansion, but Counselman and Shapiro (*28*) show that a thermal bulge could not account for capture into Mercury's 3 : 2 spin-orbit resonance (*29*). Evidently, a prior permanent bulge must have existed.

The retrograde rotation of Venus is such that, to a very good approximation, the same meridian is directed toward Earth at each inferior conjunction; as in the case of Mercury, there may be large gravity anomalies on Venus which produce a resonance lock (*29*). On the other hand, Mariner 5 tracking data (*30*) suggest a small dynamical flattening for Venus, at least two orders of magnitude less than that for Earth. Such a value is probably too small to be reconciled with the observed spin-orbit resonance; thus the question of dynamical asymmetries on Venus remains open. [*Note added in proof*: T. Gold and S. Soter (private communication) have recently suggested that atmospheric tides on Venus will permit the spin-orbit resonance to be maintained by much smaller gravity anomalies than earlier theories (*29*) had required.]

The possibility that strictly local density inhomogeneities contribute to departures from hydrostatic equilibrium in such bodies is supported by the recent deduction of subsurface mass concentrations (mascons) on the moon. From Doppler shifts in Lunar Orbiter tracking data, Muller and Sjogren (*31*) detected local variations in the acceleration of the spacecraft indicative of lunar gravity anomalies. They published a map of the earthward components of these accelerations normalized to a spacecraft altitude of 100 km, if the mascons are assumed to be 50 km below the surface. Their map indicates a gravitationally rough moon with the highest accelerations correlated one-to-one with the circular maria. Table 1 lists the maximum values for the normalized accelerations over the five nearside circular maria. Large accelerations were also observed over Mare Orientale, but the maximum value is uncertain (*31*).

The discovery of lunar gravity anomalies correlated with circular basins, when combined with the fact that large circular areas are nonuniformly distributed on the moon, Mars, and perhaps Mercury (Fig. 1), led O'Leary (*32*) to suggest that mascons account for the dynamical asymmetries discussed above. In this paper we discuss this concept and its implications in some detail.

Moon

The moments of inertia of a mascon of mass m at a distance r from the lunar center are

$$A = mr^2(1 - \cos^2\phi \cos^2\lambda)$$
$$B = mr^2(1 - \cos^2\phi \sin^2\lambda)$$

and

$$C = mr^2 \cos^2\phi \qquad (1)$$

where ϕ and λ are the selenographic latitude and longitude of the mascon. The locations of the circular maria are

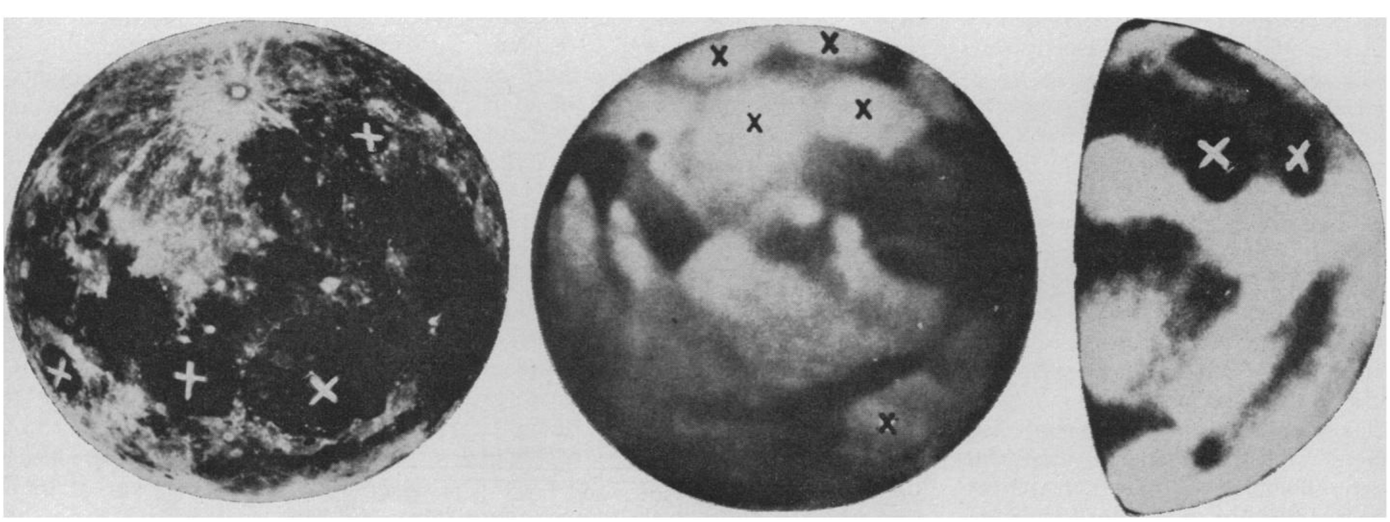

Fig. 1. Circular basins on (left to right) the moon, Mars, and Mercury. Each disk shows the South Pole pointed upward, and each basin is indicated by a cross in the center. The lunar disk is from the Photographic Lunar Atlas and shows (left to right) Maria Crisium, Nectaris, Serenitatis, Imbrium, and Humorum; the Martian disk is a photograph of the Roth Globe (*46*) showing (left to right) Thyle I, Electris, Thyle II, and Eridania near the South Pole and Elysium in the Northern Hemisphere (Table 2); and the Mercurian disk is a drawing by Camichel and Dollfus (*50*) showing (left to right) Sinus Martis and Sinus Iovis (Table 3).

generally well known, but the masses of the mascons are uncertain. However, we can estimate the relative masses of the mascons for the five nearside circular maria by assuming that the maximum spacecraft accelerations over these maria are proportional to their mascon masses (*33*). It is then possible to calculate values (Table 1) for the mascon contributions $\Delta(C-A)/m_I r^2$ and $\Delta(B-A)/m_I r^2$ by weighting differences in moments of inertia from Eq. 1 by the appropriate mass for each mascon, normalized to the value of Mare Imbrium, m_I.

The situation for most of the lunar farside cannot be assessed from the acceleration data of Muller and Sjogren because the spacecraft is in occultation (*31*). However, we have found it possible to use the spherical harmonic expansions of the moon's gravitational potential to deduce the large-scale gravity anomalies over the entire lunar surface. We have chosen to use the set of 25 coefficients of Lorell and Sjogren (*34*), which is based on observations of four Lunar Orbiter satellites, and have derived from it an equivalent mass distribution on the surface of a sphere (*35*). This is the distribution of mass which would reproduce the spatially varying part of the selenopotential, including its dependence on altitude above the surface. Figure 2 depicts the mass distribution required when the incremental mass is distributed over a spherical surface 300 km below the lunar surface; it shows large concentrations in the vicinity of Imbrium-Serenitatis, Orientale, and Nectaris despite the poor spatial resolution resulting from the use of only 25 coefficients. (A point mass described by the same set of coefficients has its mass reproduced to an accuracy of about 80 percent, but one-half of this mass will appear to lie outside a spherical cap of selenocentric half-angle 22°.)

Two more large concentrations of mass appear in Fig. 2, one in the vicinity of Mare Marginis and the other near the center of the farside disk. We have established that these are not artifacts of the spherical harmonic expansion (*36*). Their presence has some interesting implications.

First, we believe that we have discovered a partly hidden circular basin, which we have tentatively called Occultum (*36*), in the same region as the mascon near the center of the lunar farside disk. Both the size of Occultum and its mascon mass appear to be larger than those of any other basin-mascon pair, although, as with Mare Orientale, there is a question of which concentric escarpment should be considered as the basin periphery (*36, 37*). There also appears to be a large circular basin associated with the Marginis mascon (*36*). Their locations and diameters are estimated in Table 1. Except for a small mass peak in the vicinity of the nearside Southern Highlands, we confirm the association of mascons with circular basins. As a further check on the results displayed in Fig. 2, we used the same set of 25 coefficients to expand our model consisting of eight point masses buried 300 km below the surface. The resulting mass distribution mimics quite closely the observed distribution of Fig. 2. The major discrepancies are in areas south of Mare Nectaris and south of Mare Occultum, thus indicating the need for more careful investigation of these regions. We do not suggest that lunar gravity anomalies can be explained in their entirety by a model comprising eight (or ten) point masses, but such a model does seem to depict all the major features adequately.

We estimate the values of the mascon masses of Occultum, Marginis, and Orientale from integration of the distributions of Fig. 2. From an examination of various models, we have determined that the relative values for the mascon masses are insensitive to their depths beneath the lunar surface. However, some corrections in the masses are necessary because the Crisium mascon is confounded with the Imbrium-Serenitatis and Marginis peaks and the Humorum mascon is included in the Orientale peak. This complication can be resolved by use of the ratios of masses determined from the data of Muller and Sjogren (*31*). Table 1 lists the masses; we estimate their maximum error to be about 30 percent.

Table 1. Estimated parameters of the lunar circular basins and their mascons.

Circular basin	Normalized maximum acceleration* (mm/sec^2)	Basin diameter† (km)	Latitude* (deg)	Longitude* (deg)	Mascon mass (m_I)	Incremental differences in moments of inertia: $\Delta(C-A)/m_I r^2$	$\Delta(B-A)/m_I r^2$
Imbrium	2.9	674	32	−17	1.00	0.38	0.60
Serenitatis	2.1	587	25	19	0.72	.41	.47
Crisium	1.9	528	18	56	0.67	.12	− .23
Nectaris	1.2	446	−15	33	0.42	.25	.16
Humorum	0.7	459	−23	−38	0.24	.09	.05
Orientale		500–900	−20	−95	1.43	− .16	−1.24
Marginis		860‡	23‡	91‡	2.42	− .36	−2.03
Occultum		600–1600	11§	173§	4.82	4.40	4.51
Sum						5.13	2.29
						$(B-A)/(C-A)$	$= 0.45$

* From Muller and Sjogren (*31*). Accelerations are corrected for the projection on the spacecraft-Earth vector. † Derived from Baldwin (*41*), except for the Orientale, Marginis, and Occultum basins which are measured from the Lunar Farside Chart (*36*). ‡ Derived from Apollo 8 photography (*36*). § Derived from Lunar Farside Chart (*36*).

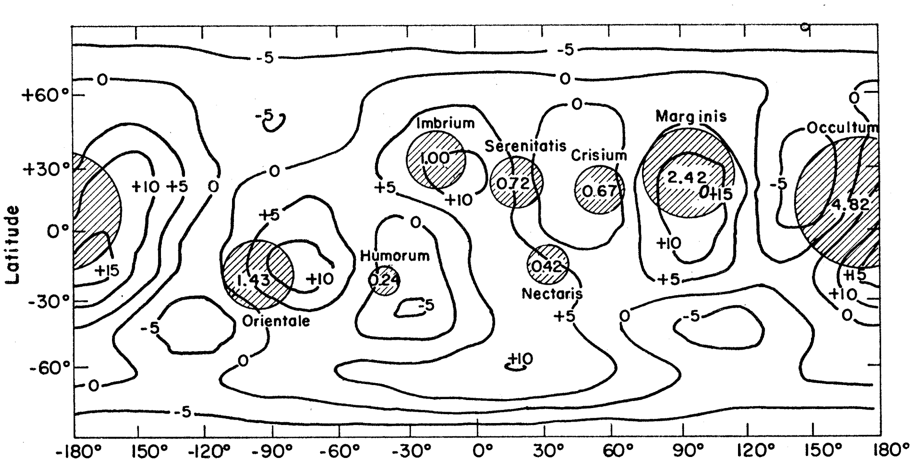

Fig. 2. The mass density corresponding to the spatially varying part of the moon's gravitational potential. Contours are in units of 10^5 g cm^{-2} referred to an arbitrary zero. The area of each basin as drawn is proportional to its estimated mascon mass from Table 1.

Since the distances of the mascons from the lunar center are roughly similar, we can now sum the mascon contributions to the moments of inertia of a moon otherwise in hydrostatic equilibrium. We obtain the values listed at the bottom of Table 1. These show that $C > B > A$, as observed, and that

$$(B - A)/(C - A) = 0.45$$

in good agreement, in view of the restricted character of our eight-mascon model, with the generally accepted value of 0.37 (*3–6*).

Until now we have been concerned only with the ratio of the mascon masses. We can calculate the absolute values of the masses required to produce the observed moments of inertia. Observations (*38*) of the inclination of the axis of rotation of the moon to the pole of its orbit indicate (*3–6*)

$$(C - A)/B = 6.3 \times 10^{-4}$$

From the forced physical libration in longitude arising from the attraction of Earth on the moon's equatorial bulge (*39*), Koziel (*6*) derives

$$(B - A)/C = 2.3 \times 10^{-4}$$

These values exceed by an order of magnitude those predicted from hydrostatic equilibrium and tidal distortion (*5, 12*). Taking for the lunar gyration constant

$$B/M_☽R_☽^2 = C/M_☽R_☽^2 = 0.40$$

corresponding to a homogeneous sphere, we derive for the nonequilibrium components

$$(C - A)/M_☽R_☽^2 = 2.4 \times 10^{-4}$$

and

$$(B - A)/M_☽R_☽^2 = 0.8 \times 10^{-4}$$

where $M_☽$ and $R_☽$ are the lunar mass and radius.

Unless the mascons are at depths of many hundreds of kilometers—an improbable occurrence (*31, 40*)—we can combine these observed values for $(C - A)/M_☽R_☽^2$ and $(B - A)/M_☽R_☽^2$ with the sums (Table 1) to find $m_I = 4 \times 10^{-5} M_☽$. This is the mass required for the Imbrian mascon if the nonequilibrium components of the lunar moments of inertia were due solely to the distribution of the eight mascons.

For comparison, Conel and Holstrom (*40*) have constructed two models which roughly fit the observed spacecraft accelerations for a traverse of Mare Serenitatis—a sphere at a depth of 200 km and a series of near-surface disks of varying diameters extending to 600 km, the approximate size of Mare Serenitatis. The masses necessary to produce the accelerations in the two cases are $m_I \simeq 5 \times 10^{-5} M_☽$ and $m_I \simeq 4.3 \times 10^{-5} M_☽$. In view of the uncertainties in the data, this constitutes rather good quantitative agreement between the mascon masses derived from the acceleration data and those estimated from our eight-mascon model. Further refinements in the selenopotential and acceleration data will very likely reveal many smaller mascons (for example, in the large circular basins Korolev, Kibalchich, and Smythii on the farside) and provide increased precision in their masses, depths, and distributions.

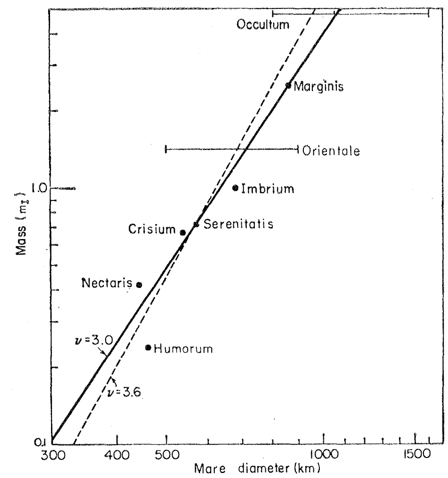

Fig. 3. Basin diameters as a function of mascon mass for the eight mascons listed in Table 1. The exponents $\nu = 3.0$ and $\nu = 3.6$ comprise two possible mass-diameter scaling laws.

As a check on the consistency of the eight-mascon model, we require from lunar spin-orbit coupling theory that the axis pointing toward Earth (the *A*-axis) be the actual least axis of the principal moments of inertia. This requirement is reasonably satisfied by our eight-mascon model. An interesting implication is that, after each event which formed the principal mascons, the lunar globe physically reoriented itself, directing a new axis of least moment of inertia toward Earth. The lunar *A*-axis would be near its present *B*-axis if the proposed Mare Occultum mascon were absent; in that case either Mare Orientale or Mare Marginis would be directed toward us, instead of the familiar "man in the moon."

One provocative consequence of our analysis is that the mascon masses are roughly proportional to the $\nu = 3.0$ to 3.6 power of their basin diameters (Fig. 3). This is expected from energy-diameter scaling laws for craters (*41*), provided we accept the hypothesis (i) that the mascons consist entirely of the impacting planetesimals and that the velocities of impact are similar. This mechanism implies collective formation of the circular basins from the same population of impacting objects. But many other hypotheses of mascon origin would also predict mascon masses that follow a diameter-cubed scaling law. Some examples are: (ii) phase changes subsequent to impact and differentiation resulting in a higher-density crater fill (*42*); (iii) a discontinuous increase in the density of the basin material produced by impact shock; (iv) integrated edge effects associated with isostatic compensation of the basins, or isostatic overcompensation; and (v) infall and upwelling of material from hydrostatic pressure which produces a convex basin floor (the deep crater formed immediately after impact will collapse and inertia may carry the debris above the surrounding level by the necessary 3 km). Conel and Holstrom's disk model (*40*) for the mascons is consistent with most of these mechanisms (*43*). A variety of other hypotheses have been advanced recently to explain the nature of the mascons (*40, 44*). [*Note added in proof*: Recently, Gilvarry (*44a*) has suggested that mascons are produced by sedimentation processes into circular depressions characterized by partial isostatic compensation. In this case as well, the same mass-diameter scaling law holds.]

Serious alterations of the orbits of circumlunar manned spacecraft might occur when they pass over the mascons. For example, mission planners should make certain that accelerations caused by passes over the Occultum region—unavoidable in equatorial orbits—do not alter a spacecraft's orbit beyond the mission constraints. The Occultum mascon could drop the spacecraft ~ 1 km closer to the lunar surface for altitudes of ~ 100 km; successive passes can amplify this effect (*45*). Special care should be taken in missions which plan orbits that "graze" the lunar surface and in rendezvous of space vehicles in lunar orbit.

Finally, the four major basin areas, Orientale, Imbrium-Serenitatis, Marginis, and Occultum, are well distributed around the equatorial plane of the lunar sphere. Thus, there is little evidence that the nearside of the moon was involved in any special way in the formation of the circular basins. On the other hand, there may be some significance attached to the preferential location of mascons roughly along a great circle near the equator.

In summary, we see that both the low-order spherical harmonics of the lunar gravitational potential and local Lunar Orbiter accelerations indicate that mascons associated with large circular basins can account for the bulk of the dynamical asymmetries of a moon which is otherwise in hydrostatic equilibrium.

Mars

Maps of Mars (*46*) also suggest the presence of several large circular areas (Fig. 1); their locations and sizes are summarized in Table 2. It has been argued (*25, 47*) that these bright areas are lowlands analogous to lunar circular basins. In any case there are no dark areas of comparable dimensions, and we assume that these circular bright areas are in fact similar to the dark lunar maria (*48*). There is a definite tendency for these areas to be polar; accordingly, their associated mascons would make a larger contribution to the mean equatorial moment of inertia

$$A = mr^2(1 + \sin^2\phi)/2$$

than to the polar moment of inertia

$$C = mr^2 \cos^2\phi$$

(Thus $C - A$ reverses sign for latitudes above 37°.) Therefore, as for the moon, mascons on Mars would tend to correct the apparent deviations from hydrostatic equilibrium evident in the discrepancy between optical and dynamical oblatenesses.

We now calculate the anticipated contribution of Martian mascons to the observed differences in moments of inertia. We again take the masses to be proportional to the $\nu = 3.0$ to 3.6 power of the basin diameters and scale from the lunar data. The resulting masses of the Martian mascons are much larger than those associated with the lunar circular maria because of the much greater dimensions of the Martian circular bright areas. As in the lunar case, we sum the contributions of each area and obtain

Table 2. Estimated parameters of suspected Martian circular bright areas.

Area (*46*)	Latitude (deg)	Diameter (km)
Arcadia	45	2000
Tempe	40	2000
Elysium	25	2000
Isidis Regio	20	1000
Neith Regio	35	1000
Baltia	65	700
Hellas	−45	2000
Ausonia	−45	2000
Eridania	−45	1300
Electris	−48	1600
Thyle I	−70	1100
Thyle II	−70	1100

$$(C - A)/m_I r^2 \approx -40 \pm 8$$

for the range of scaling laws. The negative value is required to bring the dynamical flattening into accord with the optical oblateness. Note that this value for the $C - A$ moment of inertia difference is in the opposite sense and one or two orders of magnitude greater than the corresponding lunar value. Taking $m_I \approx 4 \times 10^{-5} M_☾$, we find for the estimated contributions of mascons to the Martian difference in moments of inertia

$$(C - A)/M_♂ R_♂^2 \approx -2 \times 10^{-4}$$

where $M_♂$ and $R_♂$ are the Martian mass and radius.

We now compare these values with that necessary to explain the discrepancy in oblateness. From the data of Woolard (*17*), MacDonald (*4*) derives from the dynamical flattening

$$(C - A)/M_♂ R_♂^2 = 2 \times 10^{-3}$$

On the other hand, the measured optical oblateness (*18, 19*) and the usually assumed optical figure yield

$$(C - A)/M_♂ R_♂^2 \simeq 5 \times 10^{-3}$$

The discrepancy is $\sim -3 \times 10^{-3}$, a factor about 15 greater in absolute value than our values predicted by scaling from the Imbrian mascon. However, we do not expect the coefficient of the scaling law necessarily to be the same on Mars as on the moon. In hypothesis (i) or in Gilvarry's (*44a*) hypothesis for mascon origin, the assumption that typical impact velocities on Mars are one-quarter of the values indicated for the moon would in itself account for the entire factor. In hypotheses (ii) through (v), comparable decrements can be attributed to greater depths and densities of mare fill material for Mars than for the moon. It is also possible that large circular basins—Martian analogs of Occultum—lie undiscovered because of erosion and poor contrast. Finally, we should not neglect the contribution to the optical oblateness from isostatically compensated continental equatorial highlands (*24, 25*) nor the consequences of the observation of optical oblateness being an overestimate, as discussed in the first section of this paper. If the optical oblateness is an overestimate, the agreement with the mascon figure is improved. In either case, Martian mascons can be invoked to explain the observed departures of the dynamical figure from a Mars in hydrostatic equilibrium.

Table 3. Estimated parameters of suspected circular basins on Mercury.

Feature (*50*)	Latitude (deg)	Longitude (deg)	Diameter (km)
Sinus Martis	−15	135	1000
Sinus Iovis	−18	170	1000
Sinus Maiae	−22	195	1000

An implicit assumption of the present work is that the maria bright areas are analogous to the lunar mascon basins. It is commonly held that these lunar basins are "lowlands"—of lower average elevation than the surrounding highlands. There is evidence that the Martian bright areas are also lowlands. Although there is a suggestion of smaller circular dark areas on Mars, most of these areas are near the limit of resolution available to Earth-based observers, so that circularity can be neither confirmed nor denied. On the other hand, there can be little doubt about the approximate circularity of bright areas such as Hellas, Elysium, and Eridania. Even if the small, possibly circular, dark areas were to be mascon basins, their contributions to the Martian asymmetry would be negligible compared to those of the large circular bright areas. The Martian mascons predicted here have masses ~ 100 times the corresponding lunar values. The distances of closest approach of the Mariner flybys of Mars during 1969 and of the Mariner 1971 orbiters of Mars are intended to be ~ 2000 km. Thus there seems to be a significant probability that the predicted Martian mascons can be detected, if they are present, from observations of spacecraft acceleration in the relatively near future.

Mercury

Unfortunately, visual observations of Mercury are too inaccurate to permit unambiguous detection of large circular areas. However, there is general agreement that three "relatively circular" dark areas (*49, 50*) 1000 km in diameter exist (Table 3). In fact, Chapman's map of Mercury, based on 130 drawings and photographs, shows these areas to be the "most prominent markings" (*49*). Photometric, polarimetric, and microwave observations indicate that the surface of Mercury closely resembles the lunar surface. This would suggest that Mercury's dark spots are genetically similar to the lunar circular maria. Using the definition of Camichel and Dollfus (*50*), that the plane of zero longitude contains the sun's center at the first perihelion passage of 1950, we see that these three areas are located between longitudes 130° and 210° near latitude $-20°$. Thus, the three dark areas lie well within the region of the predicted bulge so that mascons associated with them might account for the asymmetries in Mercury's dynamical figure.

We again estimate the contribution that mascons would make to the asymmetry. In this case we are interested in differences between the equatorial moments of inertia, $B - A$, imposed by the requirement that the A-axis points toward the sun at each perihelion passage (*26*). For simplicity we neglect the small component due to tidal distortion and assume that the planet is otherwise symmetrical in B and A. The calculation of masses does not depend critically on the choice of scaling laws because the features are comparable to lunar circular maria (but are sensitive to the largest assumed impact velocities or densities and depths of the mare fill). Using Eq. 1, we can calculate the quantities $\Delta(B - A)/m_I r^2$. Since $C \simeq 0.4 M_☿ R_☿^2$, where $M_☿$ and $R_☿$ are the mass and radius of Mercury, we derive

$$(B - A)/C \approx 1 \times 10^{-4}$$

from $m_I \approx 4 \times 10^{-5} M_☾$ and from the scaling laws discussed above. These values correspond to a nonnegligible probability (~ 0.3) of capture of Mercury into a resonance lock with the sun (*29*). Thus, in the case of Mercury, three circular maria near the A-axis may quantitatively account for an asymmetry large enough to produce the observed resonance.

Earth and Venus

This discussion leads to the question of mascons in Earth. Large-scale terrestrial gravity anomalies are very small compared to the lunar values. This does not imply an absence of large mascons over all geological time, because isostatic compensation and inward migration of the high-density material could have caused mascons to disappear. It would be interesting to search for the remains of large circular basins on Earth and to correlate them with residual gravity anomalies.

Venus remains a mystery in the analysis because we cannot yet detect circular basins (although detailed radar mapping may soon change this situation). Goldreich and Peale (*29*) predict

$$(B - A)/C \gtrsim 10^{-4}$$

for any reasonable capture probability into its suspected spin resonance with Earth. However, since tracking data from Mariner 5 (*30*) now indicate a much smaller value of $(B - A)/C$, it is possible that mascons have initiated the resonance lock but have subsequently mixed into the planet by processes similar to those suggested for Earth. We speculate that Earth and Venus are "hot" objects which exhibit subcrustal plastic flow and undergo isostatic adjustment to an equilibrium state after the acquisition of a mascon, whereas the less massive moon, Mercury, and Mars are "cold" objects with no significant subcrustal plastic flow and are capable of retaining mascons near their surfaces. Since much more outgassing is expected on hot than on cold terrestrial planets, an inverse correlation between relatively dense atmospheres and mascons is expected and appears to be the case, even when corrections for relative atmospheric escape rates are included.

Conclusion

Large circular basins seem to be footprints of subsurface mass concentrations. In the case of the moon, this is obvious from Lunar Orbiter results; it is also suggested in the cases of Mars and Mercury. These mascons exhibit a nonuniform surface distribution which can both qualitatively and quantitatively explain the lunar dynamical asymmetries and perhaps similar asymmetries for Mars and Mercury.

The present data are inadequate to permit distinctions among the various hypotheses as to the form and origin of mascons (*51*), but they do seem adequate to suggest that mascons are an important and pervasive aspect of planetary geophysics and solar system cosmogony. The Lunar Orbiters and comparable future planetary probes provide excellent examples of the fundamental information which can be obtained from exceedingly simple spacecraft experiments.

References and Notes

1. See, for example, F. Press, *J. Geophys. Res.* **64**, 567 (1959); D. L. Anderson, in *The Earth's Mantle*, T. F. Gaskell, Ed. (Academic Press, New York, 1967), pp. 401–410.
2. The three lunar moments of inertia are defined as follows: *A* is about an axis along the line of centers of Earth and the moon, *C* is about the axis of rotation, and *B* is about the remaining orthogonal axis.
3. H. Jeffreys, *Mon. Notic. Roy. Astron. Soc.* **122**, 421 (1961).
4. G. J. F. MacDonald, *Space Sci. Rev.* **2**, 473 (1963).
5. ———, in *Proceedings of the Caltech–JPL Lunar and Planetary Conference: September 13–18, 1965*, H. Brown, G. J. Stanley, D. O. Muhleman, G. Münch, Eds. (California Institute of Technology and Jet Propulsion Laboratory, Pasadena, 1966), pp. 77–83.
6. C. L. Goudas, *Icarus* **3**, 375 (1964); K. Koziel, *ibid.* **7**, 1 (1967).
7. H. Jeffreys, *Mem. Roy. Astron. Soc.* **60**, 216 (1915).
8. S. K. Runcorn, *Nature* **195**, 1150 (1962); ——— and M. H. Shrubsall, *Phys. Earth Planet. Interiors* **1**, 317 (1968).
9. B. J. Levin, in *Proceedings of the Caltech–JPL Lunar and Planetary Conference: September 13–18, 1965*, H. Brown, G. T. Stanley, D. O. Muhleman, G. Münch, Eds. (California Institute of Technology and Jet Propulsion Laboratory, Pasadena, 1966), pp. 61–76; *Proc. Roy. Soc. London Ser. A* **296**, 266 (1967).
10. H. C. Urey, in *Vistas in Astronomy*, A. Beer, Ed. (Pergamon Press, London, 1956), vol. 2, pp. 1667–1680; *The Planets* (Yale Univ. Press, New Haven, 1952); G. J. F. MacDonald, *J. Geophys. Res.* **67**, 2945 (1962).
11. H. Jeffreys, *Mon. Notic. Roy. Astron. Soc. Geophys. Suppl.* **4**, 1 (1937); *The Earth* (Cambridge Univ. Press, London, ed. 4, 1959); *Proc. Roy. Soc. London Ser. A* **296**, 245 (1967).
12. Z. Kopal, *An Introduction to the Study of the Moon* (Reidel, Dordrecht, Holland; Gordon and Breach, New York, 1966).
13. ———, *Proc. Roy. Soc. London Ser. A.* **296**, 254 (1967).
14. ———, *Icarus* **4**, 173 (1965).
15. H. C. Urey, W. M. Elsasser, M. G. Rochester, *Astrophys. J.* **129**, 842 (1959); V. S. Safronov, *Vop. Kosmogonii Akad. Nauk SSSR* **7**, 59 and 121 (1960).

J. A. O'Keefe and W. S. Cameron, *Icarus* **1**, 271 (1962).

17. E. W. Woolard, *Astron. J.* **51**, 33 (1944).
18. A. Dollfus, *Compt. Rend. Acad. Sci. Paris* **255**, 144 (1962).
19. G. de Vaucouleurs, *Icarus* **3**, 187 (1964).
20. G. P. Kuiper, in *The Atmospheres of the Earth and Planets*, G. P. Kuiper, Ed. (Univ. of Chicago Press, Chicago, ed. 2, 1952), chap. 12.
21. G. de Vaucouleurs, *Physics of the Planet Mars* (Faber and Faber, London, 1954).
22. D. G. Rea, in *Proceedings of the Caltech–JPL Lunar and Planetary Conference: September 13–18, 1965*, H. Brown, G. T. Stanley, D. O. Muhleman, G. Münch, Eds. (California Institute of Technology and Jet Propulsion Laboratory, Pasadena, 1966), pp. 209–238.
23. P. Gierasch and R. M. Goody, *Planet. Space Sci.* **16**, 615 (1968).
24. H. C. Urey, *Phys. Rev.* **80**, 295 (1950).
25. C. Sagan and J. B. Pollack, *Smithsonian*

Observ. Spec. Rep. 244 (1966); *J. Geophys. Res.* **73**, 1373 (1968); C. Sagan, J. Pollack, R. M. Goldstein, *Astron. J.* **72**, 20 (1967).
G. Colombo, *Nature* **208**, 575 (1965); ——— and I. I. Shapiro, *Astrophys. J.* **145**, 296 (1966).
27. H.-S. Liu, *Science* **159**, 306 (1968).
C. C. Counselman and I. I. Shapiro, *ibid.* **161**, 602 (1968).
29. P. Goldreich and S. J. Peale, *Astron. J.* **71**, 425 (1966); *Annu. Rev. Astron. Astrophys.* **6**, 287 (1968).
30. J. D. Anderson, L. Efron, G. E. Pease, *Astron. J.* **73**, S162 (1968).
31. P. M. Muller and W. L. Sjogren, *Science* **161**, 680 (1968).
32. B. T. O'Leary, *Nature* **220**, 1309 (1968).
33. The proportionality of the maximum spacecraft accelerations with the mascon masses would arise from Newton's law of gravitation for similar mascon depths and distributions beneath each circular mare.
34. J. Lorell and W. L. Sjogren, *Science* **159**, 625 (1968).
35. E. W. Hobson, *The Theory of Spherical and Ellipsoidal Harmonics* (Cambridge Univ. Press, London, 1931), p. 151.
36. M. J. Campbell, B. T. O'Leary, C. Sagan, *Science* **164**, 1273 (1969).
37. R. B. Baldwin, *Astron. J.*, in press.
38. S. T. Habibullin, *Sov. Astron. AJ Engl. Transl.* **2**, 622 (1958).
39. A. A. Yavokin, *Trans. Int. Astron. Union* **8**, 231 (1952).
40. J. E. Conel and G. B. Holstrom, *Science* **162**, 1403 (1968).
41. E. M. Shoemaker, R. J. Hackman, R. E. Eggleton, *Interplanetary Correlation of Geologic Time* (U.S. Geological Survey, Washington, D.C., 1961); R. B. Baldwin, *The Measure of the Moon* (Univ. of Chicago Press, Chicago, 1962).
42. F. Press, personal communication.
43. We also point out that uncompensated escarpments surrounding the circular maria may contribute significantly to the distribution of mass. For example, Muller and Sjogren's map (*31*) shows a positive gravity anomaly centered at the Altai escarpment.
44. J. G. Stipe, *Science* **162**, 1402 (196 J. A. O'Keefe, *ibid.*, p. 14 R. B. Baldwin, *ibid.*, p. 14 H. C. Urey, *ibid.*, p. 1408.
44a. J. J. Gilvarry, *Nature* **221**, 732 (1969).
45. C. Oesterwinter, *Space Res.* **6**, 999 (1966). Newspaper reports by D. Kirkman (Scripps-Howard News Service, 26 December 1968) indicate that the lunar orbits of Apollo 8 were perturbed by mascons. The spacecraft was "dragged . . . almost one-third of a mile (toward the moon's surface) per revolution" and the extent of this acceleration was greater than NASA had anticipated, leading to the "suspicion that undetected (mascons) may be buried under the Moon's hidden side." Thus, the Apollo 8 orbital data seems to support our conclusion made when this paper was submitted for publication (1 month prior to the Apollo 8 mission). We await a detailed analysis of the orbits for a more accurate description of the accelerations.
46. The circularities, locations, and sizes of Martian bright areas (Table 2) are deduced from the following maps of Mars: a Roth globe (obtained from F. R. Engineering and prepared under the guidance of G. de Vaucouleurs), the Mars Planning Chart (Army Map Service), the MEC-1 prototype map (U.S. Air Force Aeronautical Chart and Information Center under the guidance of E. C. Slipher), the North American Aviation map of Mars (prepared under the guidance of A. Dollfus), and the International Astronomical Union map of Mars. Many basins that we have selected are only approximately circular—as is indeed the case for the "circular" maria on the moon.
47. D. G. Rea, *Nature* **200**, 114 (1963); *ibid.* **201**, 1014 (1964); R. A. Wells, *ibid.* **207**, 735 (1965); B. T. O'Leary and D. G. Rea, *Science* **155**, 317 (1967).
48. C. R. Chapman, J. G. Pollack, C. Sagan, *Smithsonian Astrophys. Observ. Spec. Rep. 268* (1968).
C. R. Chapman, *Earth Planet. Sci. Lett.* **3**, 381 (1967); D. P. Cruikshank and C. R. Chapman, *Sky Telescope* **34**, 24 (1967).
50. H. Camichel and A. Dollfus, in *Findings on Planetary Surfaces and Atmospheres from a Study of the Photographic Collections of the IAU Planetary Data Center at Meudon*, part I (Final Report of U.S. Air Force contract AF-61(052)-873, Observatoire de Meudon, France, 1967).
51. There is a possible categorization of mascon models into those in which there is a net gain of matter during the impact event, and those in which there is a net loss of matter. In a recent study by A. H. Marcus (*Icarus*, in press) it is suggested that impacts into the moon by objects with a velocity at great distances from the moon of 1 or 2 km/sec led to a net gain of matter; higher velocities led to a net loss. The value of the critical velocity depends on the bonding of the lunar surface material. The above numbers assume unbonded quartz sand. For better-bonded material, the critical velocities are considerably higher. It seems likely that if the lunar circular basins were produced by objects in roughly the same orbit as the moon—for example, by the final impacts in the accretion of the moon—then a net gain of matter occurred. If the basins were produced by higher velocity impacts—for example, at the present position of the moon but by asteroidal debris—then a net loss is likely to have occurred.
52. We are grateful to J. Winters and Y. S. Yang for performing calculations; to S. Soter, W. Sjogren, G. Pease, R. Tolson, H. Masursky, F. Press, T. Gold, R. Wells, S. Peale, and P. Gottlieb for helpful discussions. Supported in part by NASA grants NGL-33-010-005 and NGR-33-010-082.

Enzyme Synthesis in Synchronous Cultures

The patterns of enzyme synthesis suggest an ordered sequence of transcription throughout the cell cycle.

J. M. Mitchison

Some of the most important information on the cell cycle in recent years has come from studies of enzyme synthesis in synchronous cultures. They have thrown a new light on gene regulation in growing cells, and they have forced us to regard the cycle as a series of ordered chemical changes and not as a period of steady uniform growth between one cell division and the next. Most of the work has been done on bacteria and yeast, but there is some information on cells from higher forms, and certainly there will be more in the future. The whole of this field has not been reviewed before, but there is a good review article by Donachie and Masters (*1*) which considers the situation in bacteria.

The patterns of enzyme synthesis can be classified into two broad groups, depending on whether or not synthesis is continuous during the cycle, and each of these groups can be subdivided into two categories (Fig. 1). Most of the enzymes that have been examined (69 out of 84) are synthesized discontinuously at a particular stage of the cycle which is characteristic for each enzyme. If the enzyme is stable, the pattern is a "step" which resembles the pattern of DNA synthesis in higher cells. Each "step enzyme" therefore has its own G1, S, and G2 phase (to use the terminology for mammalian cells). A "peak enzyme" is also synthesized at one point in the cycle, but it is unstable and the activity falls off because of inactivation or breakdown of the molecule. The other, rarer group is that of enzymes which are formed continuously, and the simplest pattern is an exponential curve. Finally, a "linear enzyme" is one synthesized at a constant rate until a characteristic point in the cycle is reached, where the rate suddenly doubles. The results from most of the recent work have been divided into these categories and are listed in Tables 1 and 2.

This classification, like many others, is somewhat artificial and does not fit all cases. Unstable enzymes, for in-

The author is professor of zoology at the University of Edinburgh, Edinburgh, Scotland. This summer he is a visiting professor of zoology at the University of California, Berkeley.